SPH 3D simulation of jet break-up driven by external vibrations

Sandra Geara, Sylvain Martin, S. Adami, J. Allenou, B. Stepnik, Olivier Bonnefoy

SPH 3D simulation of jet break-up driven by external vibrations

S. Geara[a,b,c], S. Martin[a,*], S. Adami[b], J. Allenou[c], B. Stepnik[c], O. Bonnefoy[a]

[a] *Mines Saint-Etienne, Univ Lyon, CNRS, UMR 5307 LGF, Centre SPIN, F - 42023 Saint-Etienne, France*
[b] *Chair of Aerodynamics and Fluid Mechanics, Technical University of Munich, 85748 Garching, Germany*
[c] *Framatome, Cerca TM, ZI les Bérauds, BP 1114, 26104 Romans-sur-Isère, France*

Abstract

This article presents a SPH study of a liquid jet break-up, the control of which is improved by applying external vibrations. The numerical method is simple: a standard weakly compressible SPH approach where the gaseous phase is neglected. The density calculation near the free surface is based on an improved geometrical method, which was previously published by the authors. The later allows one to increase the stability of the simulations and thus to widen the range of parameters (We and Oh) compared with previous studies based on SPH. The simulation results show the capability of this approach to simulate the jet break-up phenomenon accurately. This study is a step forward, towards the simulation of liquid atomization in industrial conditions with the SPH method.

*sylvain.martin@emse.fr

Nomenclature

a_v	Acceleration due to external vibrations
A_0	Amplitude of the initial vibration (m)
$\vec{b}$	Cover vector
c_i	Color function for particle i
C	Correction coefficient for free surface density calculation
C_o	Constant parameter
c_s	Speed of sound (m/s)
Δt	Time step (s)
d	Distance to the surface (m)
D_j	Diameter of the jet (m)
D_{j_o}	Undisturbed initial diameter of the jet (m)
D_d	Droplet diameter (m)
F^ν	Viscous force (N/m^3)
F^s	Surface tension force (N/m^3)
f	Frequency (kHz)
f_{Ra}	Rayleigh Frequency (kHz)
g	External body acceleration (m/s^2)
h	Smoothing length (m)
k	Curvature $(1/m)$
k'	Wave number $(1/m)$
L_j	Length of the jet
$\tilde{L}$	Correction matrix
m	Mass (kg)
$\vec{n}$	Normal vector
$\hat{n}$	Normalized normal vector
N_d	Number of droplets
N_s	Number of satellites
Oh	Ohnesorge number
P	Pressure (Pa)
r	Position (m)
Re	Reynolds number (m)
R_c	Radius of the kernel support (m)
t	Time (s)
t_b	Break-up time (s)
v	Velocity (m/s)

v_j	Velocity of the jet (m/s)
V	Volume (m^3)
W	Kernel function $(1/m^3)$
We	Kernel function $(1/m^3)$
ζ_o	Amplitude of the initial perturbation (m)
δ_s	Surface delta function
Δx	Particle spacing (m)
Δx^0	Initial particle spacing (m)
γ	Polytropic coefficient
λ	Perturbation wavelength (m)
ν	Dynamic viscosity $(Pa.s)$
ρ	Density (kg/m^3)
ρ_0	Reference density (kg/m^3)
σ	Surface tension coefficient (N/m)

1. Introduction

The liquid jet break-up is involved in industrial atomization where the control of the droplet size is a key point. The jet break-up is the result of instabilities that grow along the liquid ligament. These instabilities are due to the competing forces, particularly surface tension and viscous forces. Lord Rayleigh was the first to propose a theoretical model for the capillary instability leading to the jet fragmentation in 1878 [1]. Later, Weber [2] included the effect of viscosity on the jet break-up and reported a linear approximation for the Rayleigh model. One possible way to control the fragmentation process is by applying external and artificial vibrations along the liquid jet or film. Experimental studies of the jet break-up [3, 4, 5, 6, 7, 8, 9] have shown that the breakup of a jet subjected to a harmonic disturbance imposed by a magnetic, acoustic or mechanical force behaves according to the Rayleigh Plateau instability analysis.

More recently, with the development of computer technology, numerical sim-

ulations of liquid jet disintegration have been performed. Richards *et al.* [10] used the Volume Of Fluid (VOF) method to study the effect of the Reynolds number on the jet break-up length and droplet size. Pan *et al.* [11] used the Level Set Method (LSM) to simulate the break-up of laminar liquid jets into still air. Using the VOF method, Deltei *et al.* [12] simulated the growth-rate dispersion relation predicted by the Rayleigh theory. Yang *et al.* [13] also used the VOF method to study the effect of forced perturbation on jet break-up for low speed and high speed regimes. Lately, Shen *et al.* [14] simulated the transition between different break-up regimes and compared the numerical data with experimental visualisations. Saito *et al.* [15] used the Lattice Boltzmann Method (LBM) to study the jet break-up problem. Menard *et al.* [16] combined LSM, VOF and Ghost Fluid Method (GFM) for the simulation of jet break-up in 3D. All previously presented methods are mesh based method that use specific interface tracking techniques and grid reconstruction process. Therefore, highly-resolved grids are required for capturing the interface accurately, which subsequently increases the calculation cost. On this basis, mesh-free numerical methods seem to be an interesting alternative for simulating jet break-up, namely Smoothed Particle Hydrodynamics (SPH) [17, 18, 19, 20].

The Smoothed Particle Hydrodynamics (SPH) is a mesh-free Lagrangian numerical method that was first introduced independently in 1977 by Lucy [21] and Gingold and Monaghan [22] to solve astrophysical problems. Since 1977, the SPH method has been significantly developed and improved to model a wide range of problems, especially in fluid dynamics. This method models a continuous fluid by discretizing it with a series of fluid particles. The continuous nature of the fluid and its properties are recovered by the spatial convolution of the physical properties of the particles by a smoothing kernel function.

Sirotkin *et al.*[18] used a corrected single phase SPH method to study viscous jet break-up and the transition from dripping to jetting for varying Weber numbers. Takashima *et al.* [17] also used SPH for 3D simulation of water break-

up. Pourabdian *et al.* [23] used the open-source SPHysics code to investigate the relation between the break-up length and the jet properties by changing Reynold and Weber numbers. Their results agreed well with corresponding experimental data. Farrokhpanah *et al.* [19] used the multi-phase SPH method to study the jet break-up phenomena and the transition between jetting and dripping regimes. More recently, Yang *et al.* [20] used a multiphase SPH model based on Riemann solvers to investigate low-speed 2D jet break-up.

The SPH method has been proven to be well designed to study accurately the jet fragmentation phenomenon. However, this approach suffers from its high computational cost. Indeed, the previous studies which simulated both gaseous and liquid phases were limited to $2D$ simulations [20, 23, 19]. The method proposed by Sirotkin [18] allows the stabilisation of single phase free surface simulation (i.e. without simulating the gaseous phase) which decrease dramatically the computational cost. This leads to very good results in 3D, although still limited to very low Webber and Reynolds numbers ($We \approx 1$ and $Re \approx 1$). In this context, the new density calculation method proposed by the authors in a previous study [24] has the potential to extend parameter range closer to industrial applications, (i.e. higher Webber and Reynolds numbers, respectively equal to 63 and 825 for the reference case). It should be noticed that similar We and Re numbers have already been reached by [17] by using an incompressible SPH method. In this article, the standard SPH approach is fully explicit and thus much simpler and scalable in a HPC framework. This method is used to study the effect of vibrations on particle size for different vibrational frequencies around Rayleigh's frequency.

2. Materials and Methods

2.1. Fluid dynamics equations

In the Lagrangian description, the Navier-Stokes equations for the conservation of mass and momentum are expressed as follows:

$$\frac{d\rho}{dt} = -\frac{1}{\rho}\nabla \cdot \vec{v} \tag{1}$$

and

$$\frac{d\vec{v}}{dt} = \vec{g} + \frac{1}{\rho}[-\nabla P + F^{\nu} + F^{s}] \tag{2}$$

where $\frac{d\vec{v}}{dt}$ is the particulate derivative.

In weakly compressible SPH, the pressure is related to the density by means of an Equation-Of-State (EOS):

$$P = \frac{\rho_0 c_s^2}{\gamma}\left[\left(\frac{\rho}{\rho_0}\right)^{\gamma} - 1\right] \tag{3}$$

The exponent γ is usually taken equal to 7 for water. The artificial speed of sound c_s is estimated based on a scale analysis of the Navier-Stokes equation presented by Morris *et al.* [25] to limit the admissible density variations..

2.2. Rayleigh-Plateau instability

The break-up of a liquid jet occurs as a result of the uncompensated surface tension force. To better understand this instability, we consider that the jet is subjected to microscopic disturbances that are superimposed. Some of these disturbances tend to decay, while other will grow in time with different growth rates. The behavior of these disturbances over time is a function of its wave number. The disturbance will eventually be dominated by the mode having the maximal growth-rate leading to the disintegration of the jet into droplets. The linear stability analysis shows that, for low Ohnesorge number, the droplet diameter and the wavelength of maximum growth rate are independent of the

material properties. They only depend on the jet diameter and its velocity [1].

The frequency of the droplets production is obtained by:

$$f = \frac{v_j}{\lambda} \tag{4}$$

where v_j is the jet velocity and λ is the disturbance wavelength. Assuming that one droplet per wavelength will be produced, the droplet diameter can be obtained by a mass balance:

$$\lambda \frac{\pi}{4} D_j^2 = \frac{\pi}{6} D_d^3 \Longrightarrow D_d^3 = \frac{3}{2} \lambda D_j^2 \tag{5}$$

where D_j stands for the initial jet diameter and D_d the diameter of the droplets.

The optimal wavelength that leads to the largest growth rate can be obtained from the dispersion relation proposed by Weber [2]:

$$w(k') = \sqrt{\frac{\sigma}{\rho R_j^3}} \left[\sqrt{\frac{(k'R_j)^2 - (k'R_j)^4}{2} + \frac{9Oh^2 (k'R_j)^4}{4}} - \frac{3Oh(k'R_j)^2}{2} \right] \tag{6}$$

where $k' = \frac{2\pi}{\lambda}$ denotes the wave numbers. Thus, the wave-number corresponding to the most unstable perturbation is obtained by:

$$k'_{max} R_j = \frac{1}{\sqrt{2}} \left[1 + \frac{3Oh}{\sqrt{2}} \right]^{\frac{-1}{2}}$$

Using Equation 4, the Rayleigh frequency, for low Oh number is expressed as: $f_{Ra} = 0.2219 \frac{v_j}{D_j}$.

Considering this mechanisms, it is possible to control the droplet formation by imposing a controlled disturbance, for example introducing an additional sinusoidal force. In such applications, the size of the droplets can be chosen in a certain range depending on the applied frequency. Sakai *et al.* [26] showed that the optimal conditions for obtaining a uniform droplet size distribution depend on the velocity of the jet and the applied frequency of the vibrations. There exists a cut-off frequency beyond which the effect of the vibrations will no longer

dominate the fragmentation process. To avoid this situation, the disturbance wavelength must be larger than the circumference of the jet. In other words, there can be no significant effect of the vibrations if the frequency is higher than $f_c = \frac{v_j}{\pi D_j}$.

2.3. Numerical model

2.3.1. SPH equations

The basic idea behind SPH is to discretize a continuous domain with a set of particles, each one with its own mass and other physical properties that can evolve with time. Interpolation using kernel functions is at the head of the SPH method. In this context, the value of any field function f at a position r can be computed with the kernel function W via:

$$f(\vec{r}) \approx \sum_{j}^{N} \frac{m_j}{\rho_j} f(\vec{r}_j) W(|\vec{r} - \vec{r}_j|, h), \tag{7}$$

where m_j and r_j are the mass and position of particle j, respectively. W represents the weighting kernel function with the smoothing length h.

Various SPH formulations can be obtained depending on the assumptions and purpose of the simulation [27]. In our study, we used the formulation proposed by Adami *et al.* [28]. The momentum equation is written as:

$$\frac{d\vec{v}_i}{dt} = \frac{1}{m_i} \sum_{j} -(V_i^2 + V_j^2) \left[\tilde{p}_{ij} \vec{\nabla} W_{ij} + \frac{2\nu_i \nu_j}{\nu_i + \nu_j} \frac{\vec{v}_{ij}}{r_{ij}} \frac{\partial W_{ij}}{\partial r_{ij}} \right] + \frac{\vec{F}_i^{(s)}}{m_i} \tag{8}$$

where V and ν are the particle volume and dynamic viscosity, respectively. $\vec{v}_{ij} = \vec{v}_i - \vec{v}_j$ is the relative velocity between particles i and j and $r_{ij} = |\vec{r}_i - \vec{r}_j|$ is the distance between the two particles. $\vec{F}_i^{(s)}$ denotes the surface tension force applied on particle i, and $\tilde{p}_{ij} = \frac{\rho_i p_j + \rho_j p_i}{\rho_i + \rho_j}$ is the averaged pressure between particle i and j.

The Continuum Surface Force (CSF) approach is used to model the surface tension force ($\vec{F}_i^{(s)}$). This approach was initially proposed by Brackbill [29] and then extended by Morris *et al.* [30]. The surface tension force is expressed as a volumetric force applied only to particles close to the interface:

$$\vec{F}^{(s)} = -\sigma k \vec{n} \delta_s \tag{9}$$

where σ is the surface tension.

Here, δ_s is the surface-delta function used to smooth the surface tension force over a band of particles near the free surface, $\vec{n}$ is the normal vector and k is the curvature. When dealing with free-surface flows, the standard SPH approximations suffer from the lack of full support for particles near the free surface. In consequence, additional corrections should be applied to accurately estimate the normal direction and the curvature of the interface. In this work, the correction matrix for the kernel gradient [31] is used for the calculation of the local normal vector, and the curvature is estimated following Sirotkin *et al.* [18]. The equations are as follow.

The color function for the particle i is:

$$c_i = \sum_j \frac{m_j}{\rho_j} c_j^0 W_{ij}$$

where c_j^0 is equal to 1. for the liquid particles. Then, one can define the correction matrix such as:

$$\tilde{L}_i = \sum_j V_j W_{ij} \otimes \vec{r}_{ij}$$

This leads to the following expression for the corrected kernel gradient:

$$\vec{\nabla} \tilde{W}_{ij} = L_i^{-1} \vec{\nabla} W_{ij}$$

Finally, one can express the normal vector and δ function:

$$\vec{n}_i = \sum_j V_j (\frac{1}{c_i} + \frac{1}{c_j}) \vec{\nabla} \tilde{W}_{ij}$$

$$\delta_i = \Lambda ||\vec{n}_i||$$

where Λ is a constant parameter which was chosen equal to 5. in 3D. Then, the curvature k is calculated following:

$$k_i = \sum_j V_j (\vec{n}_j - \vec{n}_i) \vec{\nabla} \tilde{W}_{ij}$$

The full details for the surface tension force calculation are given in [24].

2.3.2. SPH density calculation

The calculation of the density close to the free surface is very challenging for SPH simulations with a single phase, due to the lack of full support domain. In this work, an improved method developed by the authors and published previously [24] is used. It was found that this method is able to improve the stability of SPH simulations with strong topological changes like in atomization. The density of a free surface particle i is corrected with a geometric factor that takes into account the curvature of the free surface and the distance between particle i and the surface, as described in [24]. Therefore, the density is calculated as follows:

$$\rho_i = C_i m_i \sum_j W_{ij} \tag{10}$$

where C_i is expressed in 3D by:

$$C_i = \frac{1}{1 - \frac{\int_{V_{empty}} W(r) dV}{\int_{V_{SD}} W(r) dV}} \tag{11}$$

Then, using the cubic spike kernel allows one to find an analytical solution to the integrals. This kernel has been chosen for its capability to prevent insta-

bility against compression which is the main source of numerical instability in the simulation of single phase jet break-up [18]. Hence, the previous equation becomes:

$$C_i = \frac{(\frac{d}{h} - 3)^5(-4(\frac{d}{h})^2 + 3\delta + 28\frac{d}{h}\frac{1}{kh} + 42\frac{1}{kh} + 27)}{20412(\frac{d}{h} - \frac{1}{kh})} \tag{12}$$

V_{SD} and V_{empty} are the volume of the support domain of particle i and the empty volume represented by the missing particles at the free surface (i.e. within the gaseous phase), respectively. d represents the distance between particle i and the nearest surface particle, and k is the curvature of the surface at that location.

2.3.3. Continuous inlet flows

For present work, we chose to adopt the buffer zone approach for a continuous inlet flow, similarly to [32, 33]. The domain is divided into two parts: the buffer zone containing inflow particles and fluid particles. In the buffer zone, taken as wide as the kernel radius, the particles are forced to move along the pre-defined streamlines. All particles on a specific streamline have the same velocity, chosen in order to have a given velocity profile (linear, parabolic). Once an inflow particle leaves the buffer zone, it becomes a fluid particle and a new inflow particle is created at the entrance of the inflow zone. The new fluid particle will then move freely according to the SPH equations. The sketch explaining the treatment of the inflow boundary conditions and the creation of new fluid particles is presented in Figure 1.

At the outlet, open boundary conditions are imposed: after the atomization, the fragmented particles will travel for a short distance in the domain and then leave it.

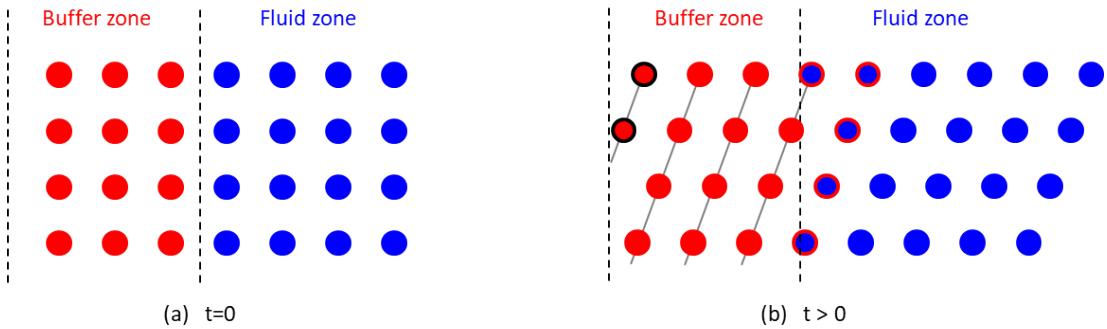

Figure 1: Sketch of the process of particle creation. Buffer particles are represented in blue and fluid particles in red. New particles created in buffer zone are identified with a black circle and buffer particles entering the fluid zone with a red circle.

2.3.4. Time integration

The time integration scheme used in this work is the kick-drift-kick scheme, also known as the velocity Verlet algorithm used by Monaghan [27]. It starts with the prediction of the intermediate velocity:

$$\vec{v}^{(t+\frac{1}{2}\Delta t)} = \vec{v}^{(t)} + \frac{1}{2}\Delta t\ \vec{a}^{(t)}. \tag{13}$$

Then, the position is updated by:

$$\vec{r}^{(t+\Delta t)} = \vec{r}^{(t)} + \Delta t\ \vec{v}^{(t+\frac{1}{2}\Delta t)}. \tag{14}$$

The new density and forces are calculated at this new position, the acceleration is deduced from Newton's second law of motion (see section 2.3.1). Finally, the velocity is updated by:

$$\vec{v}^{(t+\Delta t)} = \vec{v}^{(t+\frac{1}{2}\Delta t)} + \frac{1}{2}\Delta t\ \vec{a}^{(t+\Delta t)}. \tag{15}$$

For stability reasons, the time step Δt should be limited. It must respect the following condition [30]: $\Delta t \leq min\{0.25\ \frac{h}{c_s+v_{ref}}; 0.25\left[\frac{\rho h^3}{2\pi\sigma}\right]^{1/2}; 0.125\ \frac{\rho h^2}{\nu}; 0.25\left[\frac{h}{g}\right]^{1/2}\}$

2.3.5. Vibrations

One possible way to control the fragmentation process of a liquid jet break-up is to apply external vibrations by means of a sinusoidal acceleration in the form:

$$a_v(t) = A_0(2\pi F)^2 sin(2\pi F t) \tag{16}$$

where A_0 and F are the amplitude and frequency of the vibrations, respectively. This acceleration is applied in the flow direction to all the SPH particles located into the cylindrical reservoir (see subsection 2.4), excepted the one which are in the buffer zone.

2.4. Simulation set-up

The simulations have been performed for a water jet in the Rayleigh break-up regime. Water is issued from a vertical capillary with an internal diameter $R_j = 150\mu m$. The boundary condition used in the simulation is the generalized static wall proposed by [34] which requires that the wall be made of three layers of fixed solid particles, as shown in Figure 2.

The major issue with this representation of the wall is the very approximate shape of a cylinder coming from the Cartesian grid on which solid particles are placed. This point is discussed further in the results section. It should be noticed that alternatives exist in the literature to generate initial packing that follows the curvature at the boundaries (see [35] for example). However, this kind of algorithm was not implemented yet in the code so it was decided to stick to the Cartesian grid version.

An initial velocity profile is imposed on liquid particles as follows:

$$v_z(r) = v_{max}\left(1 - \frac{r^2}{R_j^2}\right) \tag{17}$$

where v_{max} and R_j are the maximum output velocity and the orifice radius, respectively. The simulation set-up is presented in Figure 2. Three dimension-

less parameters (two independent) are generally used to described the system: $Re = \frac{\rho v_{ref} D_j}{\mu}$, $Oh = \frac{\mu}{\sqrt{\rho \sigma D_j}}$ and $We = \frac{\rho v_{ref}^2 D_j}{\sigma}$. The simulation parameters and the relevant dimensionless numbers are summarized in Table 1. According to the Re and Oh numbers, the break-up of the liquid jet follows the Rayleigh regime [36].

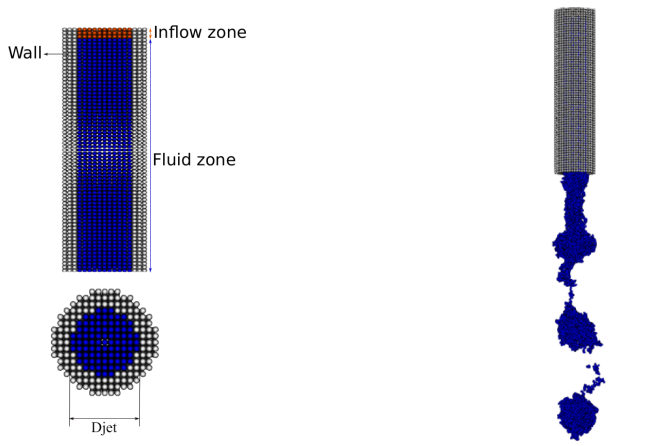

(a) Simulation set-up (b) Jet break-up

Figure 2: Water jet break-up simulation.

Table 1: Simulation parameters.

Parameter	Value
Fluid	Water
Jet diameter (D_j)	150 μm
Jet mean velocity (v_{ref})	5.5 m/s
Density (ρ)	1000 kg/m^3
Dynamic viscosity (ν)	0.001 $N.s/m^2$
Surface tension (σ)	0.072 N/m
Gravitational acceleration (g)	9.81 m/s^2
Vibration's frequency (f)	7-11 kHz
Reynolds number (Re)	825
Ohnesorge number (Oh)	0.0096
Weber number (We)	63

Finally, a convergence study in space have been led to justify the choice of Δx, which was chosen equal to 10^{-5} m. The choice of the spacial step is indeed

critical since the spacial convergence of SPH can be guaranteed only if both Δx and h tends towards 0 while the number of neighboring particles increase towards the infinite [37]. The later implies that the ratio $R_c/\Delta x$ should be increased while decreasing Δx which is very complicated to do for obvious CPU time reasons. More details are given in Appendix B.

3. Results and discussion

All the simulations presented in this paper have been run with a homemade code developed by S. Adami and based on the OpenFPM library [38]. Figure 3 represents snapshots of the jet break-up for different vibration frequencies as a function of time. As expected, the introduction of the external vibrations allows to control the breakup process. For the shown frequencies, we observe that the number of satellite particles tends to slightly decrease when increasing the vibration frequency. The break-up at the Rayleigh's frequency presents the most regular pattern results.

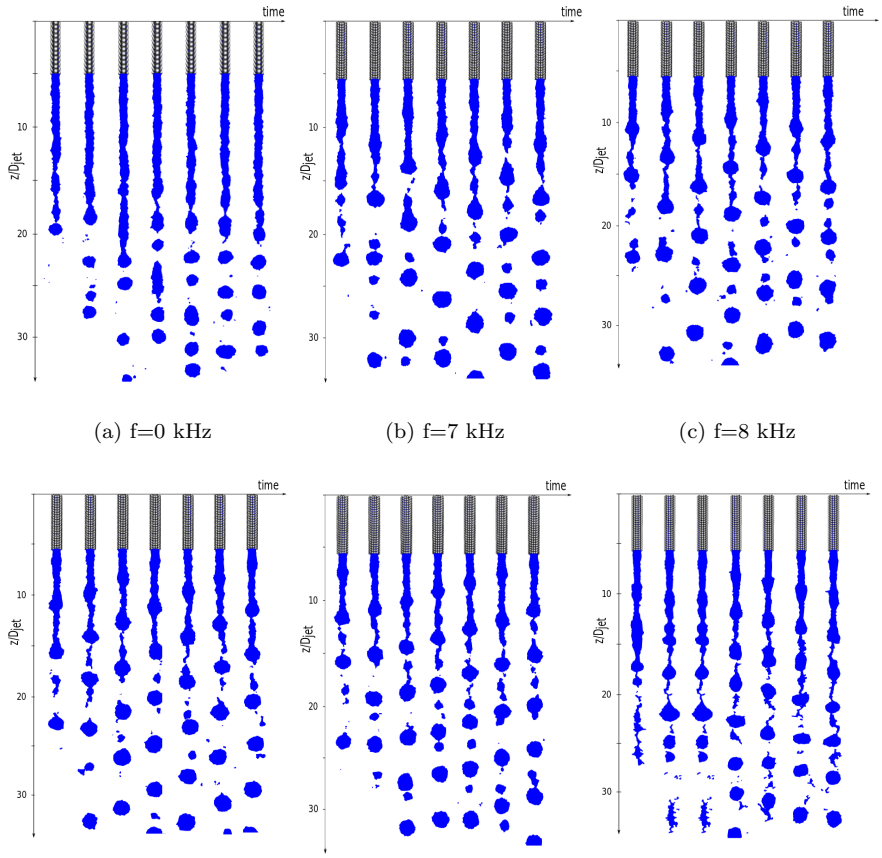

(a) f=0 kHz (b) f=7 kHz (c) f=8 kHz

(d) f=8.4 kHz (Rayleigh's frequency) (e) f=9 kHz (f) f=11 kHz

Figure 3: Snapshots of the jet fragmentation for different frequencies and times ($\Delta t = 0.2$ ms).

3.1. Particle size

For a quantitative comparison, the average diameter of the main droplets obtained by the SPH simulations is compared to theoretical prediction given by Equation 5. It should be noticed that this equation does not consider the volume of satellites. However, the later represents a very small fraction of the total droplets volume. The detailed number of droplets and satellites obtained in each simulation is given in Appendix A. The cumulative volume of satellites

represents between 0.5% and 5% of the total volume, which finally leads to an error on the theoretical diameter $\leq 2\%$.

The results are presented in Table 2 and Figure 4.

The SPH results agree very well with the theoretical droplet diameter: for the range of frequencies studied here, the mean droplet diameter tends to decrease with increasing frequency. Furthermore, the size of the satellite droplets also tends to decrease with the increase of the frequency.

Table 2: Theoretical and SPH mean droplet diameter as a function of the applied frequency.

$f(kHz)$	0	7	8	8.4	9	11
f/f_{Ra}	0	0.83	0.95	1	1.07	1.3
D_j^{Theol} (μm)	-	300	287	282	276	258
D_j^{SPH} (μm)	263	281	278	275	269	240
Standard deviation (μm) (SPH)	27	13	11.5	10.5	10	10.6
Relative Error (%)	-	7	3.3	2.6	2.5	7

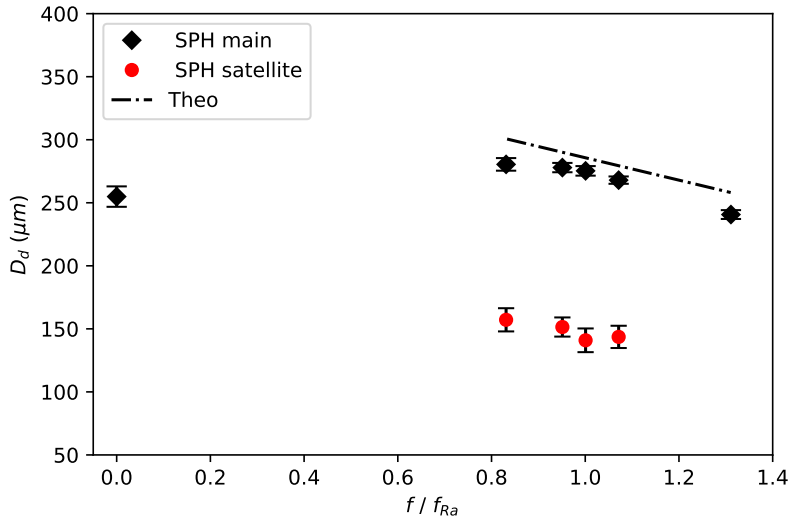

Figure 4: Theoretical and SPH data for the variation of the mean and satellite droplet diameter as a function of the applied frequency.

3.2. Break-up time

Figure 5 shows the break-up time of the first droplet as a function of the perturbation frequency. Starting from low perturbation frequencies, the break-up time decreases and then tends to increase after reaching a minimum value for the optimum frequency predicted by Rayleigh's theory. In fact, the break-up time is directly influenced by the growth rate of the disturbance considering that the jet breaks when the disturbance amplitude is equal to the jet radius. The largest growth rate (i.e. shorter break-up time) is obtained for frequencies around the Rayleigh frequency, therefore the break-up time is shortest for $f/f_{Ra} \simeq 1$. For $f \neq f_{Ra}$, the growth rate decreases resulting in an increase in the break-up time.

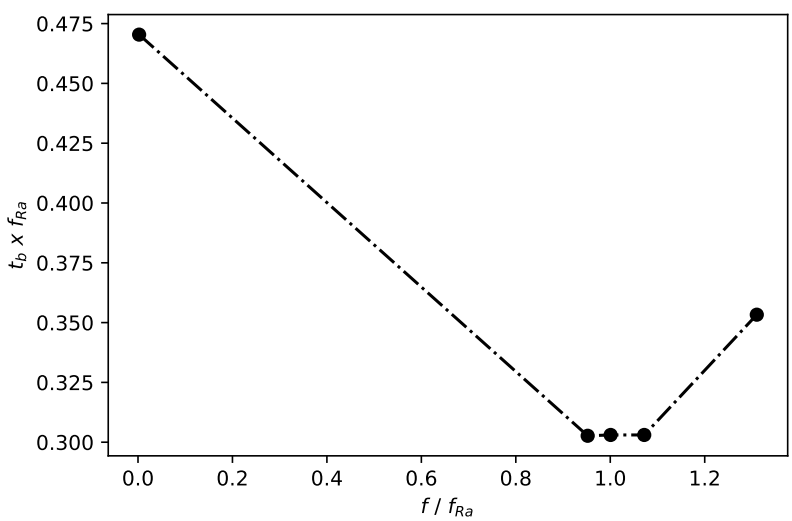

Figure 5: Break-up time of the first droplet as a function of the frequency.

Figure 3 shows that the generation of main droplets is sometimes accompanied by the formation of satellite droplets. This behavior was also reported in the literature (see for example [13, 20]). This might be explained by the experimental study conducted by Vassallo and Ashgriz [39] for liquid jet break-up. They distinguished three break-up processes: rear merge satellites, forward

merge satellites and no satellites. In the first two processes the jet breaks into a main droplet and a satellite droplet which later merges with the main droplet. In this study, the SPH simulations show that some satellite droplets merge with the main droplets on their trajectory. As shown in Figure 6, the satellite droplet merges with the main droplet within approximately two wavelengths. This means that more satellite droplets could vanish during their trajectory.

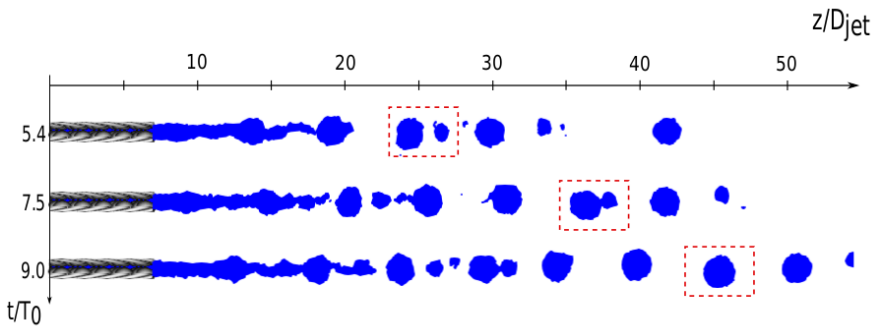

Figure 6: Satellite and main droplet merging.

3.3. Break-up distance

The dimensionless break-up distance L_j/D_j is another parameter that can be used to evaluate the quality of the simulation results. For laminar flows, the break-up distance (1) increases linearly with respect to velocity, (2) reaches a maximum and (3) decreases. Then, when the flow becomes turbulent, it increases again [40]. Different correlations can be found in the literature to calculate L_j/D_j. Most of them concern the first regime (i.e. the linear increase of L/D). The analytical expression of L_j/D_j, derived from Rayleigh theory, leads to:

$$L/D = C_o We^{0.5}(1 + 3Oh) \tag{18}$$

where C_o is a constant which was found to be ≈ 13 [41]. Then, for low Oh numbers, L_j/D_j is not a function of Oh anymore and Equation 18 becomes:

$$L_j/D_j = C_o We^{0.5} \tag{19}$$

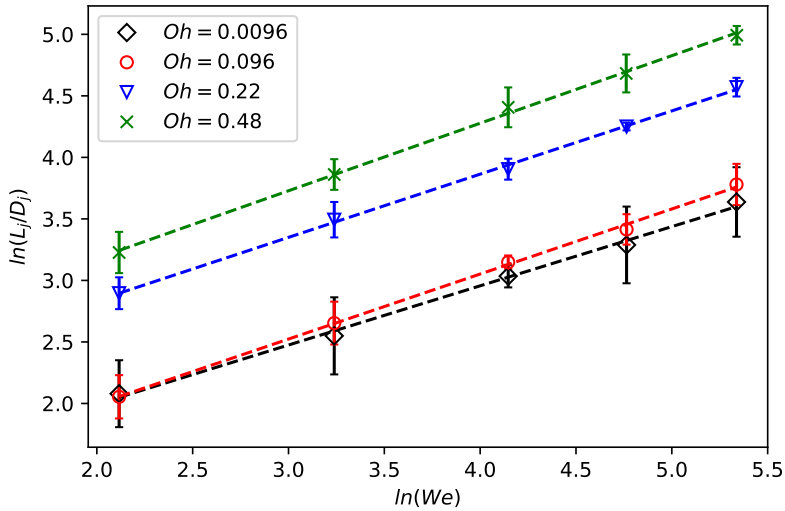

Figure 7: Determination of the dependency of ln(L/D) with respect to the ln(We) for different Oh numbers. SPH points (markers) and linear fit (dash lines)

Thus, the value of L/D depends on three parameters : We, Oh and the constant C_o. In order to validate the dependency of this 3 parameters, extra simulations without vibration have been carried out for different We and Oh numbers.The full list of parameters used in the simulations is given in Appendix A. The results are detailed below.

3.3.1. Dependency to We number

Figure 7 shows the value of $ln(L_j/D_j)$ as a function of $ln(We)$. Following Equation 18 and Equation 19, the plot should be linear with a slope equal to 0.5.

First of all, the linear fits are very good for the 4 values of Oh. Then, the slope of the fitted straight lines are respectively 0.48, 0.53, 0.51 and 0.55 for $Oh = 0.0096$, $0h = 0.096$, $Oh = 0.22$ and $0h = 0.48$. The relative error remains below 10% which is good.

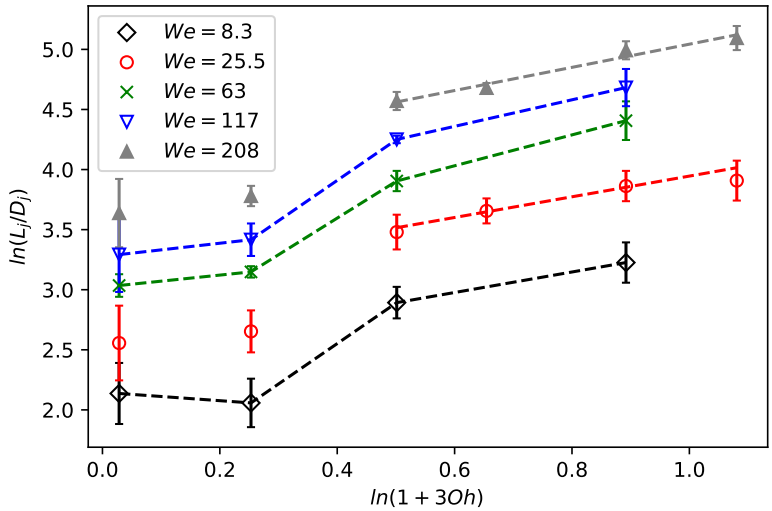

Figure 8: Determination of the dependency of $ln(L/D)$ with respect to the $ln(1+3Oh)$ for different We numbers.

3.3.2. Dependency to Oh number

Figure 8 shows the values of $ln(L_j/D_j)$ with respect to $ln(1+3.0h)$. According to the theory, two different regimes can be obtained, with a constant value for low Oh numbers (Equation 19) and a linear variation with a slope equal to 1. otherwise (Equation 18).

First of all, it can be observed that the behavior is the same for all the values of We which is in good agreement with the theory. Then, it appears that the two lower values of Oh seems to be in the constant regime while the others are in the linear regimes with respect to $ln(1+30h)$. In order to confirm the linear behavior, two extra simulations have been carried out for $We = 25.5$ and $We = 208$ in the supposed linear region which finally leads to four points to fit a straight lines for this two values of We (red and grey dashed lines on Figure 8).The fitting are quite good and the slope of the line was found to be equal to 0.86 for $We = 25.5$ and 0.96 for $We = 208$ while Equation 18 predicts a value 1. which is a quite good result.

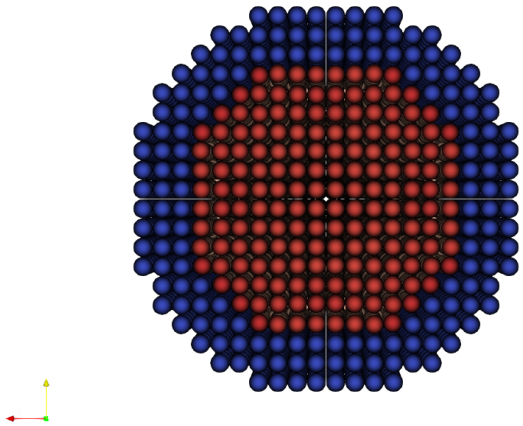

Figure 9: Cross section view the jet

3.3.3. Value of C_0

The last parameter of Equation 18 is the constant C_o. In the literature, the value of C_o is generally determined by a simple fit. However, it has a physical meaning and can be estimated with respect to the initial conditions. C_o is indeed a function of the initial perturbation amplitude ζ_0 and undisturbed diameter D_0, following the equation: $C_o = ln(\frac{D_0}{\zeta_0})$ [41]. In our simulations, the initial jet is composed of a cubic packing of SPH particles. Thus, one can assume that the main initial perturbation comes from the approximation of a circle by a cubic packing. A cross section view of the jet is given in Figure 9. Starting from this point, one can estimate that the maximum amplitude of the perturbation is about half of the spacing distance between SPH particles on each side of the jet, which leads to $C_o \approx 2.6$. It should be noticed that this value is much lower to the one proposed in the literature ($C_o = 13$) due to our very rough approximation of a circle. The comparison between the theoretical dimensionless break-up distance and the SPH results is given in Figure 10.

The SPH results are closed to the theoretical predictions, even if they don't

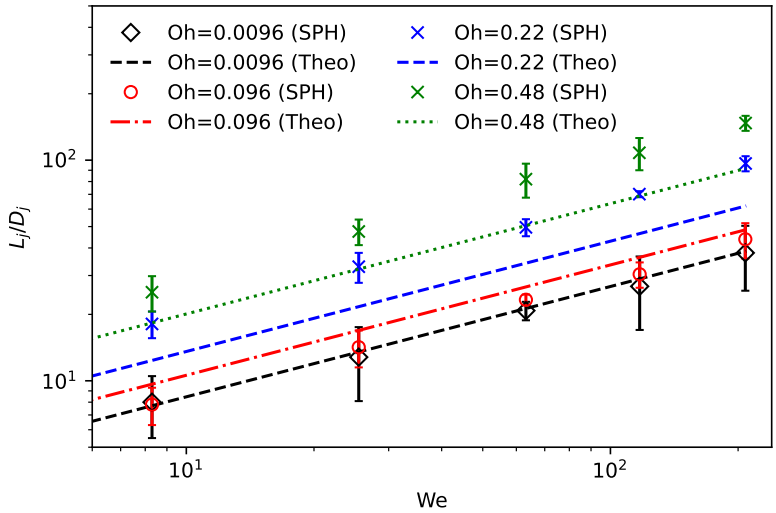

Figure 10: Break-up length with respect to We number for different Oh numbers (Oh= 0.0096, Oh=0.096 and Oh=0.48), respectively labelled as series (1), (2) ans (3). Comparison between SPH simulations and theoretical results given by Equation 18 with $C_o = 2.6$

match perfectly. However, considering the rough approximation of C_o, this results is still very satisfying. Moreover, one should notice that the determination of C_o with a fit of SPH results would require to define exactly the validity range of Equation 18 and Equation 19 with respect to the Oh number.

We can then conclude that our model gives a consistent representation of break-up distance for each of the driving parameter, Oh, We and the initial perturbation amplitude..

Finally, the break-up distance can also vary with the vibration frequency. Figure 11 presents the time history of the liquid column length L_j/D_j for the different frequencies. It can be seen that the liquid column length varies periodically with a period equal to that of the imposed vibrations. This shows that the break-up process is driven by the external mechanical solicitations. This is consistent with the numerical and experimental results published by Takashima *et al.* [17]. This result was also confirmed recently by the study of Yang [20] who showed that the period of pinch-of-length variation is equal to the vibration

period when the inlet velocity variation is large enough.

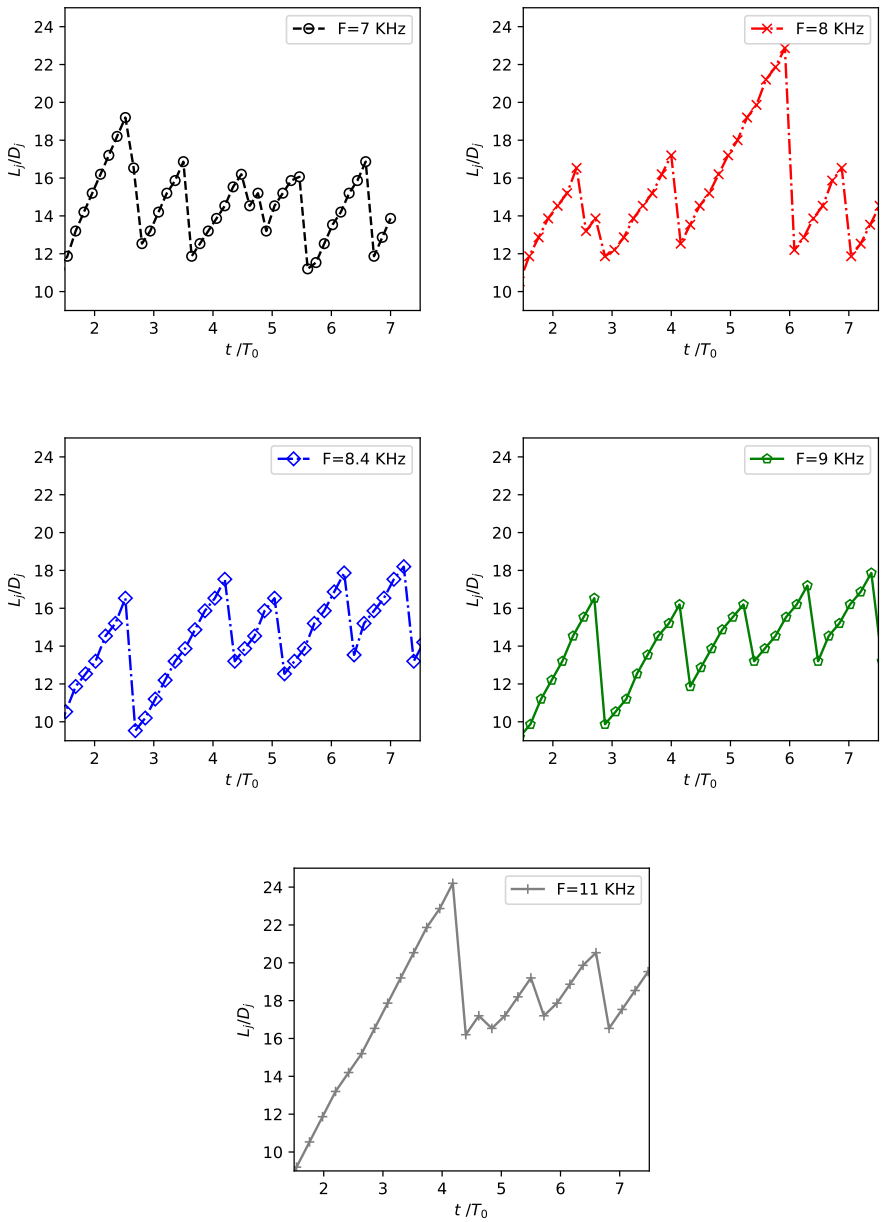

Figure 11: Variation of liquid column length as a function of time for the tested frequencies

3.4. Capability of the method, comparison with previous study

The jet breakup problem is fully defined by two dimensionless parameters, We and Oh. Sometimes, Re is also used, which is a combination of the two others ($Re = \frac{\sqrt{We}}{Oh}$). The Oh represents the competition between the viscosity and the surface tension. In numerical simulations, viscosity allows the damping of numerical instabilities. In SPH simulations, the later comes from the rough estimation of the curvature, which induces local nonphysical surface tension force. Thus, dealing with low Oh number is very challenging. This effect is even more significant for simulations in which the gaseous phase is not simulated since there is half less particles close to the surface to estimate the curvature. This is the reason why the previous paper from Sirotkin [18] presented $3D$ results with a single Oh number chosen such as $Oh = 0.9$. Physically, this would corresponds to a liquid with the density of water but a viscosity ten times higher.

In the current study, the aim was to get closer to the properties of realistic fluids. Hence, we took $We = 63$ and $Oh = 0.0096$ for the vibration study which corresponds to a jet of water with a diameter $D = 150\mu m$. and a range of parameters $We = [8; 208]$, $Oh = [0.0096; 0.48]$ for the L/D study without vibrations. Table 3 shows the comparison of We and Oh values used in the different studies since the one of Sirotkin.

Table 3: Theoretical and SPH mean droplet diameter as a function of the applied frequency.

Ref	**Gaseous particles**	**Dimension**	**We**	**Oh**
[18]	No	3D	$[0.1 - 4.]$	0.9
[23]	yes	2D	$[0.34 - 4.3]$	1.6×10^{-3}
[19]	yes	2D	$[0.1 - 1]$	$9. \times 10^{-2}$
[17]	No	3D	$[1.6; 118]$	2.5×10^{-3}
This study	No	3D	$[8 - 208]$	$[9.6 \times 10^{-3} - 0.48]$

The only $3D$ study able to deal with high We and small Oh is the one proposed by [17]. The authors use an incompressible SPH method which is slightly different from classical SPH method. Indeed, the incompressibility is ensured by an extra internal loop in which the particles are moved slightly until the density variation at each particle's position is lower than 1%. Unfortunately, since this

article is a conference paper, very few details are given on the results. Still, the results are very encouraging and their method seems to be the best alternative to simulate low viscous jets. It should be noticed that the good capability of incompressible SPH approach to simulate low viscosity free surface flow is quite logical since the biggest challenge in such simulation is to prevent the instability against compression. Conversely, in this paper we show that our density calculation method with a spike kernel is able to stabilize the simulations with the standard compressible SPH method. At the end, our kinematics conditions are quite similar and we use approximately the same number of SPH particle in the diameter of the jet(≈ 15). Moreover, our method should be faster than the incompressible method since the later requires an extra loop within each time step to maintain the incompressibility of the flow.

4. Conclusion

In this paper, we presented the numerical simulation of the vibration-controlled jet breakup. Our improved free surface single phase SPH method was shown to be able to represent accurately the different parameters of jet break-up with and without vibrations in a range of We and Re higher than previous single phase free surface SPH models. We demonstrated that our SPH approach recovers even quantitatively the important characteristic of the jet breakup: the dependency of breaking length to Weber and Ohnesorge numbers and also the influence of the vibration frequency. It can be conclude that this simple method is well adapted for the simulation of atomization of liquid within a gaseous phase.

The authors gratefully acknowledge the Gauss Centre for Supercomputing e.V. (www.gauss-centre.eu) for funding this project by providing computing time on the GCS Supercomputer SuperMUC at Leibniz Supercomputing Centre (www.lrz.de).

On behalf of all authors, the corresponding author states that there is no conflict of interest.

Appendix A. Simulations parameters and post-processing data

This appendix gives the simulation parameters for the different studies presented in the article. The simulations were run on CPU Intel Xeon Gold 6132 with 28 parallel threads. The wall clock time goes from a few days for the shorter simulations and up to 3 weeks for the longest. The paragraph bellow present the parameters for the vibration, breaking length and convergence study. In the tables, the reference case (common to all the studies) is in gray.

Appendix A.1. Vibration study

For the vibration study, 5 simulations were run with constant parameters except the vibration frequencies. The full parameter list is given in Table A.4. The size of the droplets was measured graphically with Paraview software along the 3 axes. The diameter of the droplets was then taken such as $D_d = (D_x \times D_y \times Dz)^{1/3}$. Then, a threshold was applied to distinguish satellites from regular droplets. The later was chosen such as $D < 180\mu m$. In the reference simulation without vibrations, It appears that there is only one satellite. Thus, the later was not considered in the statistics (Figure 4. Finally, for all the graphs of the article, the error bars were determined taking the student coefficient for a 95% interval. As shown in the the table, between 20 and 30 droplets were obtained in each simulation and up to 10 satellites.

Appendix A.2. Breaking-length study

For the breaking length study without vibrations, the only targeted parameter is the breaking length L_j/D_j. Since the results were very consistent, only

Table A.4: Simulation parameters for the vibration study. N_d is the number of droplets obtained in the simulation and N_s the number of satellites. The constant parameters $\rho = 1000Kg/m^3$, $g = 9.81m/s^{-2}$, $\sigma = 7.2\ 10^{-2}\ N/m$ are not given in the table.

$D_j(\mu m)$	$v_j(m/s)$	$\nu(N.s/m^2)$	$f(kHz)$	Oh	We	N_d	N_s
150	5.5	10^3	0	0.0096	63	37	1
150	5.5	10^3	7	0.0096	63	20	10
150	5.5	10^3	8	0.0096	63	28	9
150	5.5	10^3	8.4	0.0096	63	23	8
150	5.5	10^3	9	0.0096	63	32	7

a few number of droplet were necessary ($\approx 5-10$) to get the mean values with a reasonable uncertainty. The breaking length was measured graphically by the mean of Paraview software. The parameters used for each simulation and the number of droplets are given in Table A.5.

Appendix A.3. Convergence study

For the spacing convergence study (see Appendix B),the parameters are given in Table A.6.

Table A.5: Simulation parameters for the break-up length study. The constant parameters $\rho = 1000Kg/m^3$, $g = 9.81m/s^{-2}$, $\sigma = 7.2\ 10^{-2}\ N/m$ are not given in the table.

$D_j(\mu m)$	$v_j(m/s)$	$\nu(N.s/m^2)$	Oh	We	N_d
150	2	$1.\ 10^{-3}$	0.0096	8.3	6
150	3.5	$1.\ 10^{-3}$	0.0096	25.5	6
150	5.5	$1.\ 10^{-3}$	0.0096	63	7
150	7.5	$1.\ 10^{-3}$	0.0096	117	6
150	10	$1.\ 10^{-3}$	0.0096	208	6
150	2	$1.\ 10^{-2}$	0.096	8.3	8
150	3.5	$1.\ 10^{-2}$	0.096	25.5	5
150	5.5	$1.\ 10^{-2}$	0.096	63	24
150	7.5	$1.\ 10^{-2}$	0.096	117	10
150	10	$1.\ 10^{-2}$	0.096	208	7
150	2	$2.25\ 10^{-2}$	0.217	8.3	8
150	3.5	$2.25\ 10^{-2}$	0.217	25.5	10
150	5.5	$2.25\ 10^{-2}$	0.217	63	10
150	7.5	$2.25\ 10^{-2}$	0.217	117	9
150	10	$2.25\ 10^{-2}$	0.217	208	3
150	3.5	$3.2\ 10^{-2}$	0.308	25.5	8
150	10	$3.2\ 10^{-2}$	0.308	208	10
150	3.5	$5.\ 10^{-2}$	0.48	8.3	5
150	5.5	$5.\ 10^{-2}$	0.48	25.5	12
150	7.5	$5.\ 10^{-2}$	0.48	63	6
150	10	$5.\ 10^{-2}$	0.48	117	4
150	10	$5.\ 10^{-2}$	0.48	208	8
150	3.5	$6.74\ 10^{-2}$	0.65	25.5	6
150	10	$6.74\ 10^{-2}$	0.65	208	6

Appendix B. SPH and Convergence

The spatial convergence of SPH simulation for free surface flow with surface tension is a complex problem. Indeed, the convergence condition for SPH method requires (1) Δx and the smoothing length h tends towards 0 and (2) the numbers of neighboring particles tends towards the infinity. It implies that the ratio of the cutting length by the spacial discretization $R_c/\Delta x$ should be increased while decreasing Δx [37, 42].

In the standard case where R_c is kept proportional to Δx and h, the number of neighbors remain constant and the condition 2) is not fulfilled. In the other hands, increasing $R_c/\Delta x$ while decreasing Δx to increase the number of neighbors leads to a dramatic increase of CPU time due to the neighboring search

Table A.6: Simulation parameters for the spacing convergence study. The number of droplets is not given for the $\Delta x/\Delta x^0 = 0.75$ study since the simulation was too long to be reasonably . The constant parameters $\rho = 1000Kg/m^3$, $g = 9.81m/s^{-2}$, $\sigma = 7.2\ 10^{-2}\ N/m$ are not given in the table.

D_j	$v_j(m/s)$	$\nu(N.s/m^2)$	Oh	We	Δx	$\Delta x/\Delta x^0$	N_d
150	5.5	10^{-3}	0.0096	63	$1.5\ 10^{-5}$	1.5	17
150	5.5	10^{-3}	0.0096	63	$1.2\ 10^{-5}$	1.2	13
150	5.5	10^{-3}	0.0096	63	$1.1\ 10^{-5}$	1.1	21
150	5.5	10^{-3}	0.0096	63	$1.\ 10^{-5}$	1.	24
150	5.5	10^{-3}	0.0096	63	$9\ 10^{-6}$	0.9	14
150	5.5	10^{-3}	0.0096	63	$7.5\ 10^{-6}$	0.75	5

algorithm. Moreover, in a distributed memory parallel framework for HCP simulations, such as the one used in our code [38] this requires an increase of the ghost area for each thread and thus decreases the scalability of the simulation.

In this context, we tested different Δx keeping the cutting length such as $R_c = 3\Delta x = 3h$ to keep the constant the number of neighbors. The full list of parameters used in the simulations is given in Appendix A.

First of all, the breaking length L_j/D_j was compared with the theoretical value. The main point with the breaking length is its dependency to the initial perturbation with determines the value of C_0 (see subsection 3.3). As explained in this section, one of the main limit of our code comes from the cubic initial packing which does not allow a perfect representation of the cylindrical initial jet.

The initial perturbation ζ_o was estimated, for the different simulations to be $\approx \Delta x$ The theoretical value for L_j/D_j was then obtained with respect to Equation 18. The comparison between these theoretical values and the SPH results for the different Δx is given in B.12.

The graph shows that the theoretical values given by Equation 18 predict the good tendency but it does not allow to conclude about the convergence. The only outcome from that figure is the confirmation that decreasing Δx leads to a better representation of a circle, i.e. smaller ζ_o and thus greater L_j/D_j.

Another relevant piece of information concerning the convergence comes from

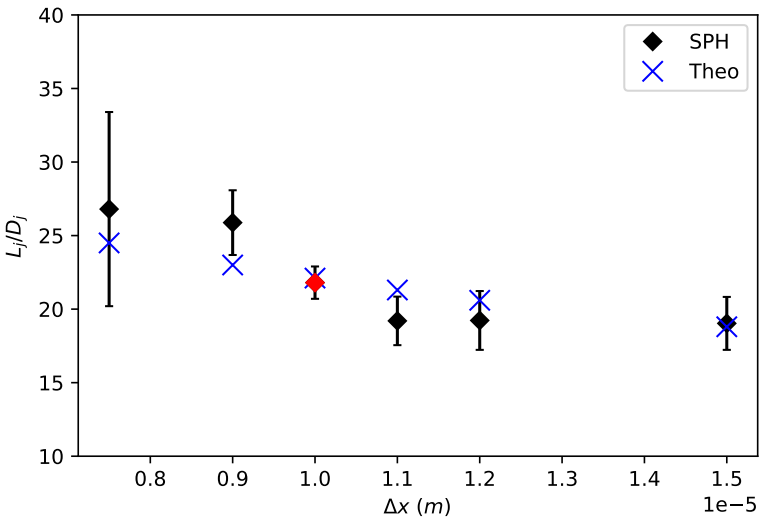

Figure B.12: Evolution of the jet break-up distance with respect to spatial resolution. The marker for the chosen resolution ($\Delta x = 1\ 10^{-5}\ m$) is in red

the snapshots of the jets. On Figure B.13, it clearly appears that the free surface is smoother when Δx decreases. The number of isolated flying particles also decreases which shows a better numerical stability of the simulation close to the interface. It is not expected that theses isolated flying particles would totally disappear when $\Delta x \to 0$ since the exact conservation of mass in SPH can still lead to the generation of a very few of them at the breaking point. However, since most of the flying particles on the figure appear along the free surface and not only at the breaking point, it can be deduced that they come from the roughness of the interface. Thus, the large decrease of their number with the spacial discretization is a good parameter to show the convergence of the model.

Finally, we chose $\Delta x = 1\ 10^{-5}\ m$ which is a good compromise : the CPU time is reasonable (about 2 weeks with 20 threads - 2.6Ghz CPU for the longest simulation of the paper), the jet break-up length is stable and the free surface is smooth and easy to define.

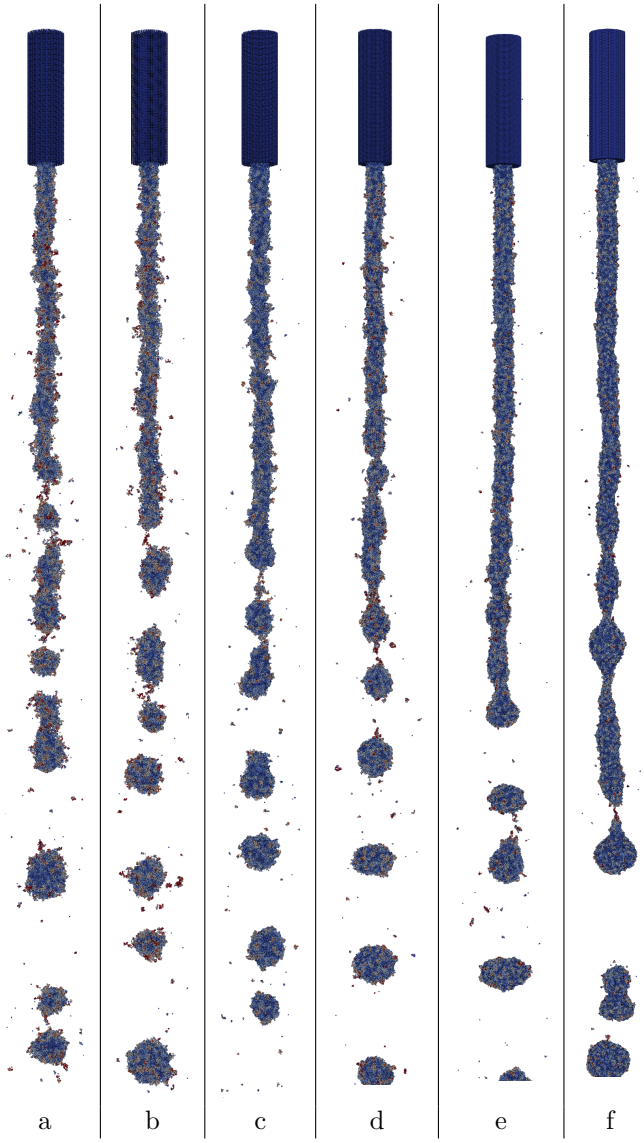

Figure B.13: Snapshops of simulation jet break-up without vibration around the chosen spacial discretization of SPH particle. The snapshots a, b, c, d, and f represent respectively $\Delta x = \{1.5\ , 1.2,\ 1.1,\ 1,\ 0.9,\ 0.75\} \times 10^{-5}$.

References

[1] L. Rayleigh, On the instability of jets, Proceedings of the London mathematical society 1 (1) (1878) 4–13.

[2] C. Weber, Zum zerfall eines flüssigkeitsstrahles, ZAMM-Journal of Applied Mathematics and Mechanics/Zeitschrift für Angewandte Mathematik und Mechanik 11 (2) (1931) 136–154.

[3] M.-C. Yuen, Non-linear capillary instability of a liquid jet, Journal of Fluid Mechanics 33 (1) (1968) 151–163.

[4] D. Rutland, G. Jameson, Theoretical prediction of the sizes of drops formed in the breakup of capillary jets, Chemical Engineering Science 25 (11) (1970) 1689–1698. doi:10.1016/0009-2509(70)80060-4.
URL https://linkinghub.elsevier.com/retrieve/pii/0009250970800604

[5] N. Ashgriz, F. Mashayek, Temporal analysis of capillary jet breakup, Journal of Fluid Mechanics 291 (1995) 163–190.

[6] C. Heinzen, I. Marison, A. Berger, U. von Stockar, Use of vibration technology for jet break-up for encapsulation of cells, microbes and liquids in monodisperse microcapsules, Landbauforschung Völkenrode, SH241 (2002) 19–25.

[7] H. González, F. J. García, The measurement of growth rates in capillary jets, Journal of Fluid Mechanics 619 (2009) 179–212. doi:10.1017/S0022112008004576.
URL https://www.cambridge.org/core/product/identifier/S0022112008004576/type/journal_article

[8] Q. Lehua, J. Xiaoshan, L. Jun, H. Xianghui, L. Hejun, Dominant Factors of Metal Jet Breakup in Micro Droplet Deposition Manufacturing Technique, Chinese Journal of Aeronautics 23 (4) (2010) 495–500. doi:10.1016/S1000-9361(09)60246-6.
URL https://linkinghub.elsevier.com/retrieve/pii/S1000936109602466

[9] T. Driessen, P. Sleutel, F. Dijksman, R. Jeurissen, D. Lohse, Control of jet breakup by a superposition of two Rayleigh–Plateau-unstable modes, Journal of Fluid Mechanics 749 (2014) 275–296. doi:10.1017/jfm.2014.178.
URL https://www.cambridge.org/core/product/identifier/S0022112014001785/type/journal_article

[10] J. R. Richards, A. M. Lenhoff, A. N. Beris, Dynamic breakup of liquid–liquid jets, Physics of Fluids 6 (8) (1994) 2640–2655. doi:10.1063/1.868154.
URL http://aip.scitation.org/doi/10.1063/1.868154

[11] Y. Pan, K. Suga, A numerical study on the breakup process of laminar liquid jets into a gas, Physics of Fluids 18 (5) (2006) 052101. doi:10.1063/1.2194936.
URL http://aip.scitation.org/doi/10.1063/1.2194936

[12] J. Delteil, S. Vincent, A. Erriguible, P. Subra-Paternault, Numerical investigations in Rayleigh breakup of round liquid jets with VOF methods, Computers & Fluids 50 (1) (2011) 10–23. doi:10.1016/j.compfluid.2011.05.010.
URL https://linkinghub.elsevier.com/retrieve/pii/S0045793011001691

[13] X. Yang, A. Turan, Simulation of liquid jet atomization coupled with forced perturbation, Physics of Fluids 29 (2) (2017) 022103. doi:10.1063/1.4976621.
URL http://aip.scitation.org/doi/10.1063/1.4976621

[14] C. Shen, F. Liu, L. Wu, C. Yu, W. Yu, Dripping, Jetting and Regime Transition of Droplet Formation in a Buoyancy-Assisted Microfluidic Device, Micromachines 11 (11) (2020) 962. doi:10.3390/mi11110962.
URL https://www.mdpi.com/2072-666X/11/11/962

[15] S. Saito, Y. Abe, K. Koyama, Lattice Boltzmann modeling and simulation of liquid jet breakup, Physical Review E 96 (1) (Jul. 2017). doi:10.1103/

PhysRevE.96.013317.
URL http://link.aps.org/doi/10.1103/PhysRevE.96.013317

[16] T. Ménard, S. Tanguy, A. Berlemont, Coupling level set/VOF/ghost fluid methods: Validation and application to 3D simulation of the primary break-up of a liquid jet, International Journal of Multiphase Flow 33 (5) (2007) 510–524. doi:10.1016/j.ijmultiphaseflow.2006.11.001.
URL https://linkinghub.elsevier.com/retrieve/pii/S0301932206001832

[17] T. Takashima, T. Ito, M. Shigeta, S. Izawa, Y. Fukunishi, Simulation of liquid jet breakup process by three-dimensional incompressible SPH method, in: Proceeding of 7th International Conference on Computer Fluid Dynamics (ICCFD7), 2012, pp. 9–13.

[18] F. V. Sirotkin, J. J. Yoh, A new particle method for simulating breakup of liquid jets, Journal of Computational Physics 231 (4) (2012) 1650–1674. doi:10.1016/j.jcp.2011.10.020.
URL https://linkinghub.elsevier.com/retrieve/pii/S0021999111006206

[19] A. Farrokhpanah, J. Mostaghimi, Application of Multiphase Particle Methods in Atomization and Breakup Regimes of Liquid Jets, in: Volume 1A, Symposia: Advances in Fluids Engineering Education; Turbomachinery Flow Predictions and Optimization; Applications in CFD; Bio-Inspired Fluid Mechanics; Droplet-Surface Interactions; CFD Verification and Validation; Development and Applications of Immersed Boundary Methods; DNS, LES, and Hybrid RANS/LES Methods, American Society of Mechanical Engineers, Chicago, Illinois, USA, 2014. doi:10.1115/FEDSM2014-21681.
URL https://asmedigitalcollection.asme.org/FEDSM/proceedings/FEDSM2014/46216/Chicago,%20Illinois,%20USA/232639

[20] Q. Yang, F. Xu, Y. Yang, L. Wang, A multi-phase SPH model

based on Riemann solvers for simulation of jet breakup, Engineering Analysis with Boundary Elements 111 (2020) 134–147. doi:10.1016/j.enganabound.2019.10.015.
URL https://linkinghub.elsevier.com/retrieve/pii/S0955799719306307

[21] L. B. Lucy, A numerical approach to the testing of the fission hypothesis, The Astronomical Journal 82 (1977) 1013. doi:10.1086/112164.
URL http://adsabs.harvard.edu/cgi-bin/bib_query?1977AJ.....82.1013L

[22] R. A. Gingold, J. J. Monaghan, Smoothed particle hydrodynamics: theory and application to non-spherical stars, Monthly Notices of the Royal Astronomical Society 181 (3) (1977) 375–389. doi:10.1093/mnras/181.3.375.
URL https://academic.oup.com/mnras/article-lookup/doi/10.1093/mnras/181.3.375

[23] M. Pourabdian, P. Omidvar, M. R. Morad, Multiphase simulation of liquid jet breakup using smoothed particle hydrodynamics, International Journal of Modern Physics C 28 (04) (2017) 1750054. doi:10.1142/S0129183117500541.
URL https://www.worldscientific.com/doi/abs/10.1142/S0129183117500541

[24] S. Geara, S. Martin, S. Adami, W. Petry, J. Allenou, B. Stepnik, O. Bonnefoy, A new SPH density formulation for 3D free-surface flows, Computers & Fluids 232 (2022) 105193. doi:10.1016/j.compfluid.2021.105193.
URL https://linkinghub.elsevier.com/retrieve/pii/S0045793021003145

[25] J. P. Morris, P. J. Fox, Y. Zhu, Modeling Low Reynolds Number Incompressible Flows Using SPH, Journal of Computational Physics 136 (1) (1997) 214–226. doi:10.1006/jcph.1997.5776.

URL https://linkinghub.elsevier.com/retrieve/pii/S0021999197957764

[26] T. Sakai, Studies on disintegration of liquid column between production of uniform size droplets by vibration method, Proc. the 3rd ICLAS, 1985 (1985).

[27] J. J. Monaghan, Smoothed particle hydrodynamics, Reports on Progress in Physics 68 (8) (2005) 1703–1759. doi:10.1088/0034-4885/68/8/R01.
URL http://stacks.iop.org/0034-4885/68/i=8/a=R01?key=crossref.c562820df517a049ca7f11d0aefe49b4

[28] S. Adami, X. Hu, N. Adams, A new surface-tension formulation for multi-phase SPH using a reproducing divergence approximation, Journal of Computational Physics 229 (13) (2010) 5011–5021. doi:10.1016/j.jcp.2010.03.022.
URL https://linkinghub.elsevier.com/retrieve/pii/S0021999110001324

[29] J. Brackbill, D. Kothe, C. Zemach, A continuum method for modeling surface tension, Journal of Computational Physics 100 (2) (1992) 335–354. doi:10.1016/0021-9991(92)90240-Y.
URL https://linkinghub.elsevier.com/retrieve/pii/002199919290240Y

[30] J. P. Morris, Simulating surface tension with smoothed particle hydrodynamics, International Journal for Numerical Methods in Fluids 33 (3) (2000) 333–353. doi:10.1002/1097-0363(20000615)33:3<333::AID-FLD11>3.0.CO;2-7.
URL http://doi.wiley.com/10.1002/1097-0363%2820000615%2933%3A3%3C333%3A%3AAID-FLD11%3E3.0.CO%3B2-7

[31] J. Bonet, T.-S. Lok, Variational and momentum preservation aspects of Smooth Particle Hydrodynamic formulations, Computer Methods in Applied Mechanics and Engineering 180 (1-2) (1999) 97–115.

doi:10.1016/S0045-7825(99)00051-1.
URL https://linkinghub.elsevier.com/retrieve/pii/S0045782599000511

[32] M. Lastiwka, M. Basa, N. J. Quinlan, Permeable and non-reflecting boundary conditions in SPH, International Journal for Numerical Methods in Fluids 61 (7) (2009) 709–724. doi:10.1002/fld.1971.
URL http://doi.wiley.com/10.1002/fld.1971

[33] I. Federico, S. Marrone, A. Colagrossi, F. Aristodemo, M. Antuono, Simulating 2D open-channel flows through an SPH model, European Journal of Mechanics - B/Fluids 34 (2012) 35–46. doi:10.1016/j.euromechflu.2012.02.002.
URL https://linkinghub.elsevier.com/retrieve/pii/S0997754612000337

[34] S. Adami, X. Hu, N. Adams, A generalized wall boundary condition for smoothed particle hydrodynamics, Journal of Computational Physics 231 (2012) 7057–7075. doi:10.1016/j.jcp.2012.05.005.

[35] A. Colagrossi, B. Bouscasse, M. Antuono, S. Marrone, Particle packing algorithm for sph schemes, Computer Physics Communications 183 (8) (2012) 1641–1653.

[36] N. Chigier, R. D. Reitz, Regimes of jet breakup and breakup mechanisms-physical aspects, Recent advances in spray combustion: Spray atomization and drop burning phenomena. 1 (1996) 109–135.

[37] E. Arai, A. Tartakovsky, R. G. Holt, S. Grace, E. Ryan, Comparison of surface tension generation methods in smoothed particle hydrodynamics for dynamic systems, Computers & Fluids 203 (2020) 104540. doi:https://doi.org/10.1016/j.compfluid.2020.104540.
URL https://www.sciencedirect.com/science/article/pii/S0045793020301122

[38] P. Incardona, A. Leo, Y. Zaluzhnyi, R. Ramaswamy, I. F. Sbalzarini, Openfpm: A scalable open framework for particle and particle-mesh codes on parallel computers, Computer Physics Communications 241 (2019) 155–177. doi:https://doi.org/10.1016/j.cpc.2019.03.007.
URL https://www.sciencedirect.com/science/article/pii/S0010465519300852

[39] Satellite formation and merging in liquid jet breakup, Proceedings of the Royal Society of London. Series A: Mathematical and Physical Sciences 433 (1888) (1991) 269–286. doi:10.1098/rspa.1991.0047.
URL https://royalsocietypublishing.org/doi/10.1098/rspa.1991.0047

[40] R. P. Grant, S. Middleman, Newtonian jet stability, AIChE Journal 12 (4) (1966) 669–678. doi:https://doi.org/10.1002/aic.690120411.

[41] N. Ashgriz (Ed.), Handbook of Atomization and Sprays, Springer US, Boston, MA, 2011. doi:10.1007/978-1-4419-7264-4.
URL http://link.springer.com/10.1007/978-1-4419-7264-4

[42] J.-P. Fürstenau, C. Weißenfels, P. Wriggers, Free surface tension in incompressible smoothed particle hydrodynamcis (isph), Computational Mechanics 65 (2020) 487–502.